Frequency shifts of Rossby waves in the inertial subranges of β-plane turbulence

Takashi Ishihara[a] and Yukio Kaneda
Department of Computational Science and Engineering, Graduate School of Engineering, Nagoya University, Chikusa-ku, Nagoya 464-8603, Japan

(Received 7 June 2000; accepted 4 May 2001)

Nonlinear interactions between waves and turbulence cause systematic frequency shifts in Rossby waves. The frequency shifts in the inertial subranges of statistically steady β-plane turbulence were examined theoretically and numerically. The theoretical analysis is based on the Lagrangian closure called the Lagrangian renormalized approximation and predicts that when the β effect is small, the frequency shifts of Rossby waves are proportional to $k_x/k^{4/3}$ in the inverse energy transfer range, while they are proportional to k_x with or without a log-correction term in the enstrophy transfer range, depending on the flow conditions, where k_x is the wave number in the eastward direction. Numerical simulations using 1024^2 grid points of forced β-plane turbulence that exhibit the inertial subranges, show fairly good agreement with theoretical predictions. © *2001 American Institute of Physics.* [DOI: 10.1063/1.1384468]

I. INTRODUCTION

In flows on a global scale, the rotation of the Earth plays a crucial role. The Coriolis force due to rotation varies with latitude, and the variation gives rise to waves, called Rossby waves, on a planetary scale. These waves interact with the background turbulence. It is necessary to fully understand these interactions in order to model flows on a global scale.

In this respect, Rhines investigated the effect of the planetary gradient of the Coriolis force by simulating two-dimensional (2-D) turbulence using the so-called β-plane model equations.[1] His numerical results showed that the excitation of Rossby waves enhances the anisotropy of the turbulence and suppresses the turbulent energy transfer to large scales (see also the review by Rhines[2]).

The interactions between turbulence and waves affect not only the intensity of turbulence, but also the frequency of the Rossby waves. In fact, numerical simulations of 2-D turbulence both in the β plane and on a rotating sphere have suggested large systematic frequency shifts in the sense of rapid westward phase propagation, especially for shorter waves (see the review by Holloway[3]). Kaneda and Holloway (hereafter referred to as KH) estimated the frequency shifts both theoretically and numerically.[4] However, their study was limited to turbulence at low or moderate Reynolds numbers.

Regarding turbulence without the Coriolis force ($\beta=0$), it has been suggested that 2-D turbulence may exhibit certain universal features, such as universal inertial ranges, at high Reynolds number. Knowledge of such universality, if any exists, may greatly facilitate the modeling of turbulence for high Reynolds numbers. Therefore, it is of interest to investigate whether there are any universal features in the interactions between Rossby waves and turbulence. Our primary purpose in this paper is to study the frequency shifts of Rossby waves in the inertial subranges of β-plane turbulence both numerically and theoretically.

Since our studies on the frequency shifts of Rossby waves in the inertial subranges of β-plane turbulence are closely related to those of 2-D turbulence with $\beta=0$, we briefly review some related studies. Dimensional analyses suggest that two kinds of inertial subranges may exist in 2-D turbulence with $\beta=0$: an inverse energy transfer range of the form

$$E(k)=C\epsilon^{2/3}k^{-5/3}, \tag{1}$$

and an enstrophy transfer range of the form

$$E(k)=C'\eta^{2/3}k^{-3}, \tag{2}$$

where $E(k)$ is the energy spectrum, C and C' are dimensionless constants, and ϵ and η are the rates of kinetic energy and enstrophy transfer per unit mass, respectively.[5–7] Kraichnan[8] suggested that because of nonlocal interaction in k space, Eq. (2) should be corrected to

$$E(k)=C_{\mathrm{K}}\eta^{2/3}k^{-3}[\ln(k/k_1)]^{-1/3}, \quad (k\gg k_1), \tag{3}$$

where C_{K} is a dimensionless constant and k_1 is a wave number at the bottom of the range.

Since the theoretical prediction of energy spectra, such as Eqs. (1)–(3), extensive studies have been made of numerical simulations to examine or confirm the existence of the inertial subranges. Numerical simulations of forced 2-D turbulence in the inverse energy transfer range[9–12] confirmed the existence of the $k^{-5/3}$ energy spectrum. It has also been reported that the spectrum may deviate from the $k^{-5/3}$ law due to the emergence of strong vortices distributed over all scales, even if the inverse energy transfer is almost k independent.[13] In the enstrophy transfer range, the spectrum of the form (3) has been shown to be robust in the sense that

[a]Electronic mail: ishihara@cse.nagoya-u.ac.jp

 © 2001 American Institute of Physics

Downloaded 19 Oct 2006 to 133.6.32.11. Redistribution subject to AIP license or copyright, see http://pof.aip.org/pof/copyright.jsp

it can be realized under various run conditions of forced 2-D turbulence (see Ref. 14 and papers cited therein).

Recent numerical simulations and a spectral closure analysis have shown that there may be another class of turbulence in which the energy spectrum scales with k like k^{-3}, as in Eq. (2), i.e.,

$$E(k)=Ak^{-3}, \tag{4}$$

in the constant enstrophy transfer range, but the prefactor A is different from that given by Eq. (2).[15] According to the simulations and analysis, this spectrum may be realized when the energy spectrum at low wave numbers $\ll k$ is so large that the dominant contributions to the enstrophy transfer rate at the similarity range come from the interactions with very low wave number modes outside the similarity range, whereas the spectrum (3) may be realized when the dominant contributions are from interactions within the range. Thus, which spectrum (3) or (4) is realized depends on the energy spectrum at low wave numbers (cf. Refs. 14 and 15). The closure analysis also suggests that there may be intermediate cases between these two classes, in which the spectrum is a mixture of the spectra (3) and (4). The energy spectrum reported recently in Ref. 16 has a bump in the low wave number range, and is consistent with the closure analysis.

In this paper, we present a series of numerical simulations with 1024^2 grid points of forced 2-D turbulence with $\beta=0$ that exhibit the inertial subrange: Eq. (1), (3), or (4). In order to numerically investigate Rossby wave propagation at the scales of the inertial subranges, we consider the cases for $\beta\neq 0$, without changing any other setting. For the theoretical estimates of the frequency shifts of Rossby waves in the inertial subranges of β-plane turbulence, we use the Lagrangian renormalized approximation (LRA),[17] which is a two-point closure theory free from any *ad hoc* parameters and is consistent with the inertial range energy spectra of Eqs. (1), (3), and (4).

The paper is organized as follows. In Sec. II, we present the basic equations and define the frequency shift of Rossby waves following KH. Section III contains numerical experiments confirming the existence of inertial subranges exhibiting Eq. (1), (3), or (4). In Sec. IV we give theoretical estimates for the frequency shifts of Rossby waves in the three kinds of the inertial subranges based on the LRA with some simplifying assumptions, and in Sec. V we compare the theoretical estimates and numerical simulations. Finally, Sec. VI is a discussion and summary.

II. BASIC EQUATIONS

The β-plane model is one of the simplest turbulence models that takes into account planetary gradients of the Coriolis force. The governing equation is

$$\frac{\partial\zeta}{\partial t}+J(\zeta,\psi)-\beta\frac{\partial\psi}{\partial x}=\nu\nabla^2\zeta, \tag{5}$$

where ψ is the stream function related to the fluid velocity as $\mathbf{u}=(\partial\psi/\partial y,-\partial\psi/\partial x)$, where $\zeta=-\nabla^2\psi$ is the vorticity, ν the kinematic viscosity, Ox and Oy are axes directed east and north, respectively, $J(\zeta,\psi)=\partial(\zeta,\psi)/\partial(x,y)$ represents the nonlinear Jacobian term, and β is the mean value of the northward gradient of the Coriolis parameter. The term representing the effect of external force is omitted in Eq. (5). In the absence of the Jacobian and viscous terms, Eq. (5) only exhibits Rossby wave propagation, while in the absence of the β term, Eq. (5) is the 2-D Navier–Stokes equation. Thus, the model is one of the simplest prototypes that contains both turbulence and wave propagation.

In geostrophic turbulence, nonlinear interactions may have significant effects on Rossby wave propagation. The linear inviscid version of Eq. (5) gives the dispersion relation for a plane transverse wave $\psi=\exp i[k_x x+k_y y-\omega_0(\mathbf{k})t]$ as

$$\omega_0(\mathbf{k})=-\beta k_x/(k_x^2+k_y^2),$$

so that the phases of Rossby waves always propagate westward, i.e., $c_x\equiv\omega_0/k_x<0$ for $\beta>0$. The nonlinear interactions may modify the frequency shift and the phase velocity. Therefore, the frequency shift is one of the simplest measures of the strength of the interactions between the waves and turbulence.

When the turbulence is statistically homogeneous and quasistationary, the Eulerian two-point two-time velocity correlation, $U(\mathbf{x}',t';\mathbf{x},t)\equiv\langle\mathbf{u}(\mathbf{x}',t')\cdot\mathbf{u}(\mathbf{x},t)\rangle$ (the brackets denote the ensemble average) depends on the arguments $\mathbf{x}',\mathbf{x},t'$, and t only through $\mathbf{x}'-\mathbf{x}(=\mathbf{r})$ and $t'-t(=\tau)$. It is convenient to introduce the Eulerian two-time correlation spectrum as

$$\begin{aligned}U(\mathbf{k},\tau)&\equiv(2\pi)^{-3}\int U(\mathbf{x}+\mathbf{r},t+\tau;\mathbf{x},t)\exp(-i\mathbf{k}\cdot\mathbf{r})d^3\mathbf{r}\\&=\langle\hat{\mathbf{u}}(\mathbf{k},t+\tau)\cdot\hat{\mathbf{u}}(-\mathbf{k},t)\rangle,\end{aligned} \tag{6}$$

where $\hat{\mathbf{u}}(\mathbf{k},t)$ is the Fourier coefficient given by $\mathbf{u}(\mathbf{x},t)=\Sigma_{\mathbf{k}}\hat{\mathbf{u}}(\mathbf{k},t)\exp(i\mathbf{k}\cdot\mathbf{x})$, and the velocity field is assumed to satisfy the periodic boundary conditions in both the x and y directions. From Eq. (5), the equation for $U(\mathbf{k},\tau)$ can be written in the form

$$\begin{aligned}&\left(\frac{\partial}{\partial\tau}+\nu k^2+i\omega_0(\mathbf{k})\right)U(\mathbf{k},\tau)\\&\quad=T(\mathbf{k},\tau)\equiv-\langle\hat{J}(\mathbf{k},t+\tau)\hat{\psi}(-\mathbf{k},t)\rangle,\end{aligned} \tag{7}$$

where $\hat{J}$ and $\hat{\psi}$ are the Fourier coefficients of the Jacobian term and the stream function in Eq. (5), respectively. Introducing the frequency spectrum $\tilde{U}(\mathbf{k},\omega)$ given by

$$U(\mathbf{k},\tau)=\int\tilde{U}(\mathbf{k},\omega)\exp(i\omega\tau)d\omega,$$

we may define the mean frequency $\overline{\omega}$ and frequency difference $\Delta\omega$ as

$$\Delta\omega(\mathbf{k})\equiv\mathrm{Re}[\overline{\omega}(\mathbf{k})]-[-\omega_0(\mathbf{k})],$$

where

$$\overline{\omega}(\mathbf{k})\equiv\int\omega\tilde{U}(\mathbf{k},\omega)d\omega\Big/\int\tilde{U}(\mathbf{k},\omega)d\omega.$$

From (7), we have

Downloaded 19 Oct 2006 to 133.6.32.11. Redistribution subject to AIP license or copyright, see http://pof.aip.org/pof/copyright.jsp

$$\Delta\omega(\mathbf{k}) = \frac{\mathrm{Im}\, T(\mathbf{k})}{U(\mathbf{k})}, \tag{8}$$

where $T(\mathbf{k}) = T(\mathbf{k},0)$ and $U(\mathbf{k}) = U(\mathbf{k},0)$.[4] In the absence of nonlinear interactions, the waves propagate westward at the so-called bare frequency $-\omega_0(\mathbf{k}) = \beta k_x/k^2$ $(\beta > 0)$, so that $\Delta\omega$ is zero. Thus, $\Delta\omega$ given by Eq. (8) is a measure of the frequency shifts induced by nonlinear interactions.

The definition (8) of the frequency shift is independent of any closure model and is therefore observable. It is different from the phase shift defined by Legras[18] on the basis of a closure model equation and used to study Rossby waves on a spherical geometry.

III. NUMERICAL EXPERIMENTS

A. Method

In order to numerically simulate the inertial subranges of Rossby wave turbulence at relatively low resolution, we use the following model equation, instead of Eq. (5),

$$\frac{\partial\zeta}{\partial t} + J(\zeta,\psi) - \beta\frac{\partial\psi}{\partial x} = F + D, \tag{9}$$

where F and D represent forcing and dissipation terms, respectively. These are described in detail below. For a doubly periodic domain of width 2π, we can express the vorticity and stream function in terms of a complex Fourier series, e.g.,

$$\psi(\mathbf{x}) = \sum_{\mathbf{k}} \hat{\psi}(\mathbf{k})\exp(i\mathbf{k}\cdot\mathbf{x}),$$

where $\mathbf{k} = (k_x, k_y)$ is any integer vector and $\hat{\psi}^*(\mathbf{k}) = \hat{\psi}(-\mathbf{k})$ to ensure the reality condition of $\psi(\mathbf{x})$. Then, the equation of motion may be cast in the form

$$\frac{d}{dt}\hat{\zeta}(\mathbf{k}) + \hat{J}(\mathbf{k}) + i\omega_0(\mathbf{k})\hat{\zeta}(\mathbf{k}) = \hat{F}(\mathbf{k}) + \hat{D}(\mathbf{k}), \tag{10}$$

where $\hat{F}(\mathbf{k})$ and $\hat{D}(\mathbf{k})$ are the complex Fourier coefficients of F and D at time t, respectively. The nonlinear term $\hat{J}(\mathbf{k})$ is computed using a staggered grid algorithm with full dealiasing.[19] The number of mesh points in real space is set to 1024^2 so that the retained wave vector domain is $k < K_{\max}$, with $K_{\max} = 481$. Time is advanced using a fourth-order Runge–Kutta method.

As in Refs. 12–15, the dissipation function $\hat{D}(\mathbf{k})$ is modeled as

$$\hat{D}(\mathbf{k}) \equiv -\alpha\hat{\zeta}(\mathbf{k}) - \gamma\zeta_{\mathrm{rms}}\left(\frac{k}{K_{\max}}\right)^{2n-2}\hat{\zeta}(\mathbf{k}), \tag{11}$$

where the linear drag coefficient α is held constant for wave number ranges $k \leqslant K_\alpha$ and is set to 0 for $k > K_\alpha$, ζ_{rms} is the rms. vorticity, which is calculated at every time step, γ is a tuning factor of order unity, and we set $n = 4$ for all the simulations. For the forcing function $\hat{F}(\mathbf{k})$, a random Markovian formulation is used, i.e.,

$$\hat{F}_n(\mathbf{k}) = A(1-R^2)^{1/2}e^{i\theta} + R\hat{F}_{n-1}(\mathbf{k}), \tag{12}$$

where the subscript of $\hat{F}_n$ denotes the nth time step of the fourth-order Runge–Kutta method, θ is a random number in $[0,2\pi]$ and is, in general, different for different $\mathbf{k}$ or n, the forcing amplitude A is held constant for all wave numbers satisfying $K_{f\,\min} < k < K_{f\,\max}$ and is set to zero for all the other wave numbers, and R is a function of the time increment Δt and the characteristic correlation time of the forcing.

Since the model equation (9) has many parameters, as shown above, we need to run some preliminary experiments at lower resolution to fix the values of the parameters for runs at a higher resolution. For this purpose, we first reproduced some of the experiments in Ref. 12 with a resolution of 256^2 or 512^2 grid points. Then, we increased the resolution to 1024^2 points, while adjusting some of the parameters in order to extend each of the inertial subranges. The values of the parameters vary from run to run, but remain constant during any given experiment. We call the runs used to produce the inverse energy transfer range (1) Series E, those for the enstrophy transfer range (2) or (3) Series Z1, and those for (4) Series Z2. The values of the parameters used in the runs are listed in Table I. The value of β was set as $\beta = 0, 5.0$, or 10.0 in each series.

The initial conditions for Series Z1 and Z2 were set to $\psi(\mathbf{x},0) = 0$, while those for Series E were given by randomly generated velocity fields with an isotropic spectrum $ak\exp(-2k/k_0)$, where $k_0 = 2.5$ and the constant a is a normalized constant chosen so that $\langle\mathbf{u}\cdot\mathbf{u}\rangle = 1$. Simulations were run until a quasisteady state was obtained. To judge whether a run was in a quasisteady state, we monitored the time dependencies of the energy and enstrophy spectra as well as the total energy and enstrophy.

B. Numerical results for the energy spectra

1. Inverse energy transfer range

Here, we examine the inverse energy transfer range obtained from Series E with $\beta = 0$, 5, and 10. Figures 1(a) and 1(b) suggest that all three runs with different values of β are in a statistically steady state after $t \approx 20$, where one time unit corresponds to about $8.5\zeta_{\mathrm{rms}}^{-1}$. After $t \approx 20$, the energy spectra fluctuate around a fixed shape, and the same occurs with the enstrophy spectra (figures omitted). The time-averaged data

TABLE I. Parameter values used in the runs: the dissipation term in Eq. (11) was determined using K_α, α, γ, and n, while the forcing term in Eq. (12) is controlled by $K_{f\,\min}$, $K_{f\,\max}$, A, R, and Δt.

	$K_{\max}$	Δt	K_α	α	γ	n	$K_{f\,\min}$	$K_{f\,\max}$	A	R
Series E	481	0.0025	6	1.0	0.5	4	320	325	1.0	0.5
Series Z1	481	0.001 25	6	1.0	0.5	4	10	14	1.0	0.5
Series Z2	481	0.005	30	1.0	0.5	4	10	14	1.0	0.5

Downloaded 19 Oct 2006 to 133.6.32.11. Redistribution subject to AIP license or copyright, see http://pof.aip.org/pof/copyright.jsp

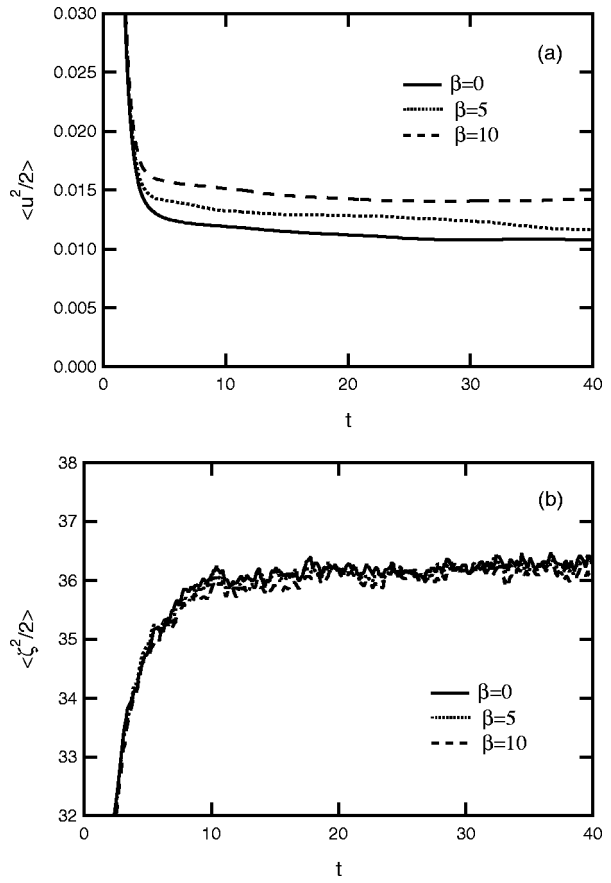

FIG. 1. Time series of the total (a) energy and (b) enstrophy for Series E.

for Series E reported below were obtained by taking time averages from $t=30$ to 40. The time-averaged energy spectra in Fig. 2 show a fairly good agreement with the scaling (1). We define the inertial energy transfer subrange as the wave number range, where the inverse energy flux defined by

$$\epsilon(k)=\mathrm{Re}\sum_{p<k}\hat{J}(\mathbf{p})\hat{\psi}(-\mathbf{p}),$$

is almost constant, independent of k. Figure 3 plots time-averaged $\epsilon(k)$'s, all of which are seen to be almost independent of k, and gives $\epsilon\sim 1.1\times 10^{-4}$ in the wave number range from $k\approx 100$ to $k\approx 200$. The values of $C(k)$

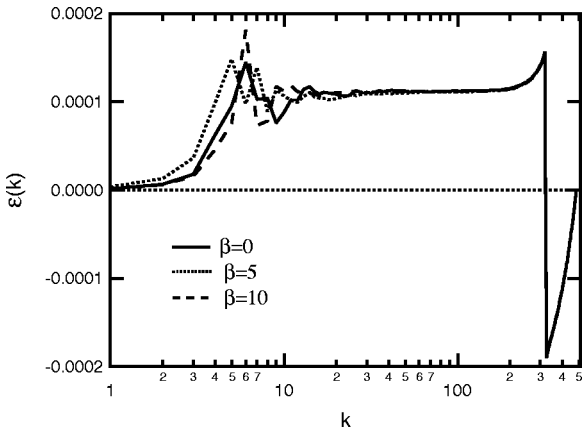

FIG. 3. Time-averaged energy flux $\epsilon(k)$ for Series E.

$\equiv\epsilon(k)^{-2/3}k^{5/3}E(k)$ for these runs are plotted in Fig. 4. Irrespective of the value of ($\beta=0$, 5, or 10), the value of C averaged over the wave number range $k\in(100, 200)$ is about 5.7, which is in good agreement with $C=5.8$ obtained numerically in Ref. 12 for $\beta=0$, and in numerical simulations by Maltrud and Vallis ($C=5.8$),[12] and is not very far from the two-point closure predictions of $C=6.69$ in the test field model (TFM)[8] and $C=7.41$ in the LRA. As shown in Figs. 2 and 3, the β effect is not pronounced in $E(k)$ and $\epsilon(k)$ in the inertial wave number range, while the effect is visible in the wave number range $k<20$.

2. Enstrophy transfer range (I)

Next, we examine the enstrophy transfer range obtained by Series Z1 with $\beta=0$, 5, and 10. The enstrophy transfer inertial range for Series Z1 may be defined as the range over which the enstrophy flux,

$$\eta(k)=-\mathrm{Re}\sum_{p<k}\hat{J}(\mathbf{p})\hat{\zeta}(-\mathbf{p}),$$

is almost constant, independent of k. Figures 5(a) and 5(b) show that both the total energy and enstrophy, which are initially zero, increase with time and almost saturate at $t\approx 40$. The enstrophy flux $\eta(k)$, as well as the energy spec-

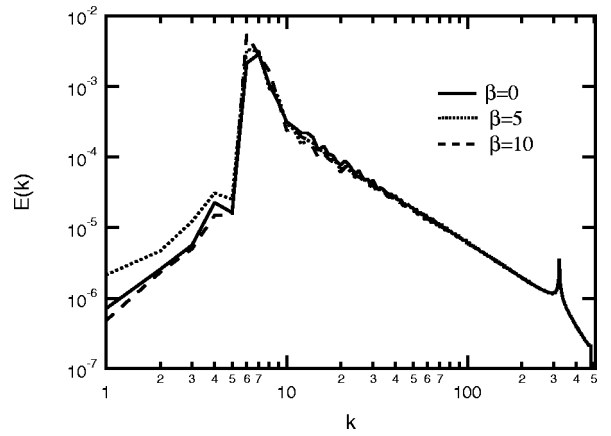

FIG. 2. Time-averaged energy spectra for Series E.

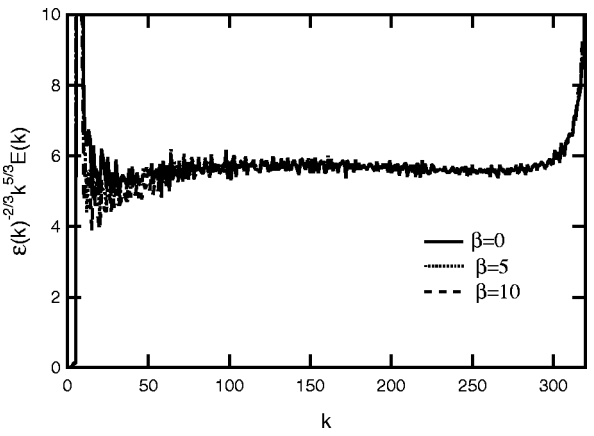

FIG. 4. Time-averaged values of $C(k)=\epsilon(k)^{-2/3}k^{5/3}E(k)$ for Series E.

Downloaded 19 Oct 2006 to 133.6.32.11. Redistribution subject to AIP license or copyright, see http://pof.aip.org/pof/copyright.jsp

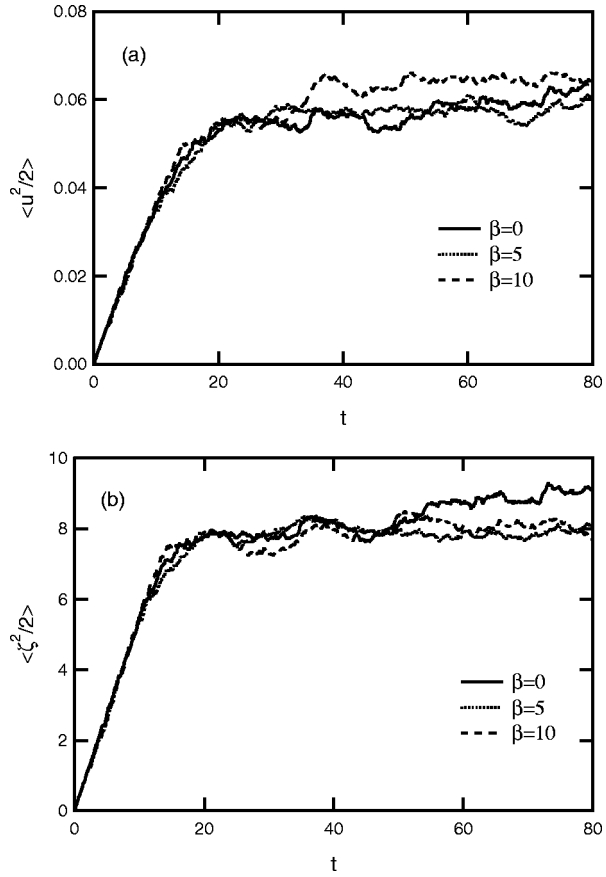

FIG. 5. Time series of the total (a) energy and (b) enstrophy for Series Z1.

trum, fluctuates around a fixed shape after $t \approx 40$. Figures 6 and 7 show time-averaged $E(k)$ and $\eta(k)$, respectively, where the time averages were taken from $t=70$ to 80 and the time interval 10 corresponds to $40\zeta_{\mathrm{rms}}^{-1}$. Figure 7 shows that the $\eta(k)$'s for $\beta=0$, 5, and 10 are almost flat over the wave number range $k \in (60, 200)$. In Fig. 6, the energy spectra for $\beta=0$, 5, and 10 are close to each other in this range. The spectrum for $\beta=0$ is identical to one reported previously and has been shown to agree well with Eq. (3) and gives $C_{\mathrm{K}} \approx 1.9$ and $k_1 \approx 18$.[14]

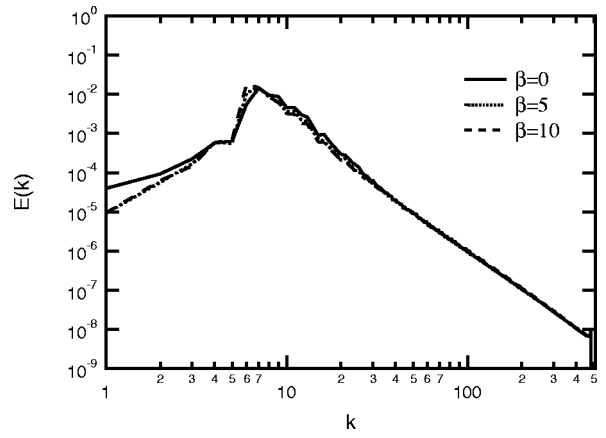

FIG. 6. Time-averaged energy spectra for Series Z1.

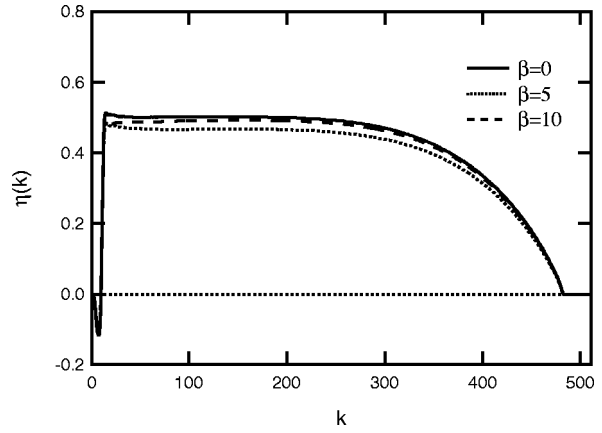

FIG. 7. Time-averaged enstrophy flux $\eta(k)$ for Series Z1.

3. Enstrophy transfer range (II)

As shown in Refs. 12 and 15, a class of 2-D turbulence exhibits the k^{-3} spectrum (4) in the enstrophy transfer range. Series Z2, in which coherent vortices are destroyed by strong infrared dissipation, corresponds to this case. The inertial subrange for Series Z2 may be defined in the same way as for Series Z1, i.e., as the range in which the enstrophy flux is almost k independent. Figures 8(a) and 8(b) show that the total energy and enstrophy only fluctuate slightly around the mean values after $t \approx 5$. However, it is also observed that the energy of the high wave number modes, which is only a

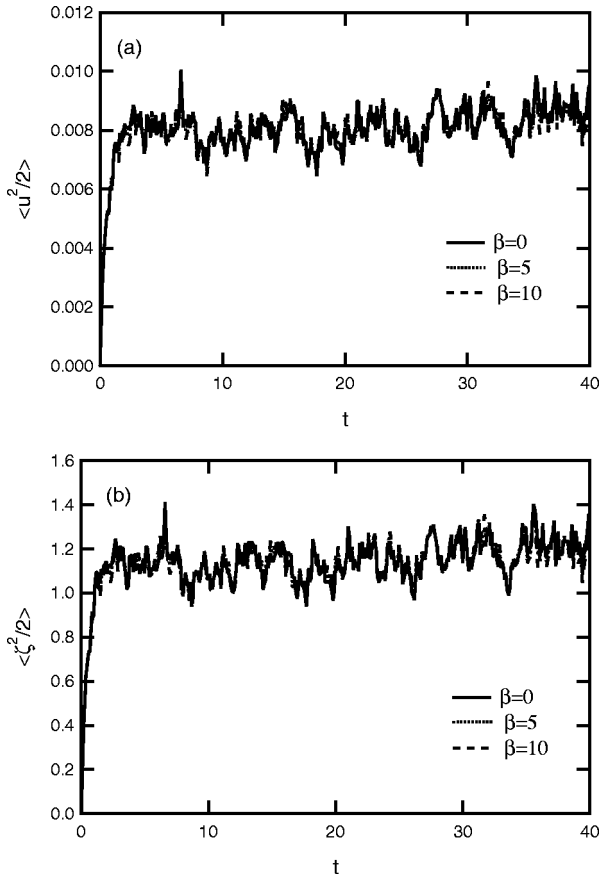

FIG. 8. Time series of the total (a) energy and (b) enstrophy for Series Z2.

Downloaded 19 Oct 2006 to 133.6.32.11. Redistribution subject to AIP license or copyright, see http://pof.aip.org/pof/copyright.jsp

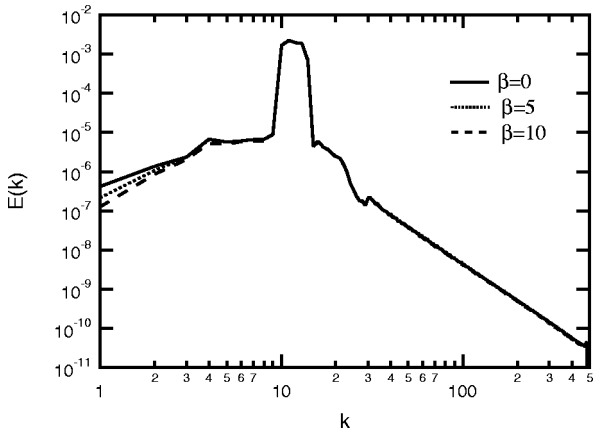

FIG. 9. Time-averaged energy spectra for Series Z2.

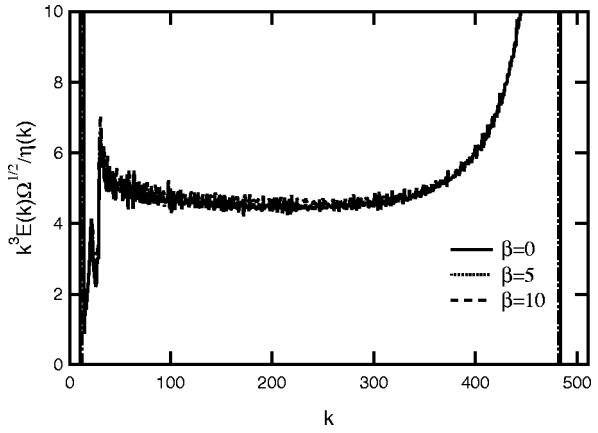

FIG. 11. Plots of $C_N(k)=k^3E(k)\Omega^{1/2}/\eta(k)$ for Series Z2.

fractional part of the total energy, does not saturate before $t \approx 20$, while the energy spectrum as well as the enstrophy flux $\eta(k)$ only fluctuate slightly around a fixed shape after $t \approx 20$ (figures omitted). Figures 9 and 10 show the time-averaged $E(k)$ and $\eta(k)$, respectively, where the average is from $t=25$ to 40 and the time interval 15 corresponds to about $23\zeta_{\mathrm{rms}}^{-1}$. Figure 10 shows that irrespective of the value of β, $\eta(k)$ is regarded as constant over the wave number range $k \in (100, 200)$. Figure 9 shows spectra close to the k^{-3} power law in this range. Analysis in Ref. 15 suggests that when there is a huge bump in the energy spectrum, as shown in Fig. 9, the spectrum in the enstrophy transfer range may be expressed as Eq. (4) with $A \approx \eta(k)/\Omega^{1/2}$. Therefore, we plot $C_N=k^3E(k)\Omega^{1/2}/\eta(k)$ as a function of k in Fig. 11, as in Refs. 12 and 15. All of the values of C_N averaged over $K \in (100, 200)$ for $\beta=0, 5$, and 10 are approximately 4.5, which shows a good agreement with the values 4.9 and 4.7 obtained numerically in Refs. 12 and 15 for $\beta=0$.

IV. THEORETICAL ESTIMATE OF $\Delta\omega$

In this section, we consider the frequency shift, $\Delta\omega$, of Rossby waves in the inertial subranges given by Eqs. (1), (3), and (4), at small β using the LRA. The application of the LRA to homogeneous turbulence obeying the β-plane model (9) yields a closed set of equations for the Lagrangian two-time correlation spectrum $Q(\mathbf{k},t,s)$ and the Lagrangian response function $G(\mathbf{k},t,s)$. When the turbulence is in a quasistationary state, the energy transfer function T is given by an equation of the form

$$T(\mathbf{k}) = \frac{1}{2}\sum_{\mathbf{p},\mathbf{q}}^{\Delta} \frac{|\mathbf{p}\times\mathbf{q}|^2}{k^2p^2q^2}\,\theta(-\mathbf{k},\mathbf{p},\mathbf{q}) \times[(p^2-q^2)^2U(\mathbf{p})U(\mathbf{q}) - 2(p^2-q^2) \times(k^2-q^2)U(\mathbf{k})U(\mathbf{q})], \tag{13}$$

where $\Sigma_{\mathbf{p},\mathbf{q}}^{\Delta}$ denotes the sum over $\mathbf{p}$, $\mathbf{q}$ satisfying $\mathbf{p}+\mathbf{q}=\mathbf{k}$. The principal difference between various closure theories comes from differences in the triple relaxation factor, θ. In the LRA, θ for homogeneous, quasistationary β-plane turbulence is given by

$$\theta(-\mathbf{k},\mathbf{p},\mathbf{q}) \equiv \int_0^{\infty} G(-\mathbf{k},\tau)G(\mathbf{p},\tau)G(\mathbf{q},\tau)\,d\tau, \tag{14}$$

where G is defined by $G(\mathbf{k},\tau) \equiv G(\mathbf{k},t,s)$ with $\tau=t-s$, and satisfies $G(\mathbf{k},0)=1$ and

$$\frac{\partial^2}{\partial\tau^2}\phi(\mathbf{k},\tau) = 2\sum_{\mathbf{p},\mathbf{q}}^{\Delta} |\hat{\mathbf{k}}\times\hat{\mathbf{q}}|^4 \frac{k^2q^2}{p^2}\exp[-\phi(-\mathbf{q},\tau)]U(\mathbf{q}). \tag{15}$$

Here, ϕ is defined by $G(\mathbf{k},\tau)=\exp[-\phi(\mathbf{k},\tau)]$, where $\hat{\mathbf{k}}=\mathbf{k}/k$ and $\hat{\mathbf{q}}=\mathbf{q}/q$. We used $\mathbf{p}\times\mathbf{q}=\mathbf{k}\times\mathbf{q}$ and $U(\mathbf{q})=U(-\mathbf{q})$. Equation (15) is to be solved under

$$\phi(\mathbf{k},0)=0 \quad \text{and} \quad \frac{\partial}{\partial\tau}\phi(\mathbf{k},\tau)\big|_{\tau=0} = i\omega_0(\mathbf{k}), \tag{16}$$

where we have omitted terms due to the dissipation terms in Eq. (11). These are assumed to be negligible in the inertial subranges under consideration. No term due to the forcing given in Eq. (12) appears in the equation for G because the forcing is assumed to be independent of the flow field.[17] In principle, the phase shift $\Delta\omega$ given by Eq. (8) can be estimated from Eqs. (13)–(16) for any energy spectrum $U(\mathbf{k})$ without introducing any further approximations. Note that the terms omitted in Eq. (16) may be significant outside the inertial subranges under consideration. For example, the α term in Eq. (11) can be nonnegligible at low wave numbers.

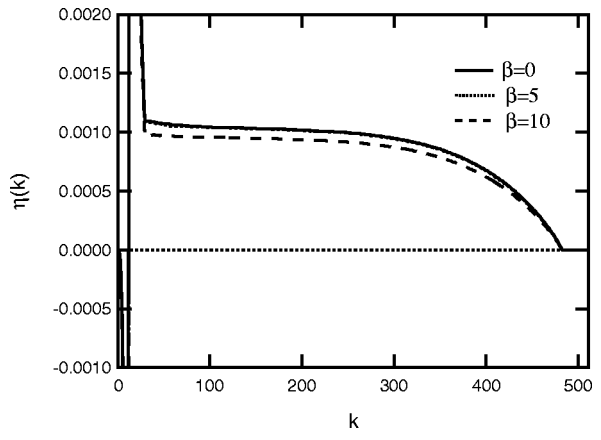

FIG. 10. Time-averaged enstrophy flux $\eta(k)$ for Series Z2.

Downloaded 19 Oct 2006 to 133.6.32.11. Redistribution subject to AIP license or copyright, see http://pof.aip.org/pof/copyright.jsp

KH estimated the LRA approximation for $T(\mathbf{k})$ by numerically solving Eqs. (13)–(15), and $(\partial/\partial\tau)\,\phi(\mathbf{k},\tau)|_{\tau=0} = \nu k^2 + i\,\omega_0(\mathbf{k})$ instead of Eq. (16), using the band-averaged as well as the time-averaged spectrum $U(k)$ instead of $U(\mathbf{k},t)$, which they obtained from (low-resolution) numerical simulations of decaying β-plane turbulence. They compared $\Delta\omega$ obtained using the LRA with the value obtained from the numerical simulation. Although large fluctuations in their simulated values of $\Delta\omega$ averaged over a short time interval made a detailed quantitative comparison difficult, the behavior of the simulated values is consistent with the LRA estimation in an averaged sense.

KH also derived a simplified approximation for $\Delta\omega$ from Eqs. (13)–(16) by introducing some assumptions. They showed that the simplified approximation agrees fairly well with the LRA without the simplifications at low and moderate Reynolds numbers. In the following, we briefly review their simplified approximation for the reader's convenience, and then apply it to the inertial subranges under consideration.

Let $T^<(\mathbf{k}|K)$ be the contribution from the interactions among modes $(\mathbf{k},\mathbf{p},\mathbf{q})$ in Eq. (13) with p or $q<K$ and let $\phi(\mathbf{k},\tau)$ be expanded for small τ as

$$\begin{aligned}\phi(\mathbf{k},\tau) &= \phi_R(\mathbf{k},\tau) + i\,\phi_I(\mathbf{k},\tau)\\ &= [A(\mathbf{k})\tau^2 + \cdots] + i[\,\omega_0(\mathbf{k})\tau + B(\mathbf{k})\tau^3 + \cdots],\end{aligned} \tag{17}$$

where

$$A(\mathbf{k}) = \sum_{\mathbf{p},\mathbf{q}}^{\Delta} |\hat{\mathbf{k}}\times\hat{\mathbf{q}}|^4 \frac{k^2q^2}{p^2} U(\mathbf{q}), \tag{18}$$

$$B(\mathbf{k}) = -\frac{\beta}{3}\sum_{\mathbf{p},\mathbf{q}}^{\Delta} |\hat{\mathbf{k}}\times\hat{\mathbf{q}}|^4 \frac{k^2q_x}{p^2} U(\mathbf{q}). \tag{19}$$

These are from Eqs. (15), (16), and $\phi(\mathbf{k},0)=0$. Then, with the following simplifying assumptions, as shown in KH:

I. There exists a wave number K for which $E \equiv (1/2)\,\Sigma_{\mathbf{q}} U(\mathbf{q}) \sim (1/2)\,\Sigma_{q<K} U(\mathbf{q})$ and

$$\mathrm{Im}\,T(\mathbf{k}) \sim \mathrm{Im}\,T^<(\mathbf{k}|K), \quad \text{for } |\mathbf{k}| \gg K.$$

II. The β effect is small, so that the anisotropy of the energy spectrum is weak, i.e.,

$$U(\mathbf{k}) \sim U(k).$$

III. $A(\mathbf{q})/[2A(\mathbf{k})]$, $|C(\mathbf{q})|/[2A(\mathbf{k})]$, and $|\omega_0(\mathbf{q})|/[2A(\mathbf{k})]$ for $k \gg q$ are small, so that

$$\mathrm{Im}\,\theta(-\mathbf{k},\mathbf{p},\mathbf{q}) \sim -\gamma(\mathbf{k})\,\omega_0(\mathbf{q}), \quad \text{for } k\sim p \gg q, \tag{20}$$

where $C(\mathbf{q}) = B(\mathbf{q})/\omega_0(\mathbf{q})$ and

$$\gamma(\mathbf{k}) = \int_0^\infty \tau \exp[-2A(\mathbf{k})\tau^2]\,d\tau, \tag{21}$$

an approximate expression of $\Delta\omega$ for small β may be given by

$$\Delta\omega(\mathbf{k}) = \frac{\mathrm{Im}\,T(\mathbf{k})}{U(\mathbf{k})} \sim -\frac{\beta\hat{k}_x\gamma(\mathbf{k})E}{4}\left(\frac{1}{U(k)}\frac{\partial[k^2U(k)]}{\partial k}\right). \tag{22}$$

In general, the expression (22) can be used for $U(\mathbf{k})$, provided that $U(\mathbf{k})$ is compatible with these three assumptions.

A. Inverse energy transfer range

When $\beta=0$, the LRA yields Eq. (1) and G in the form

$$G(k,t,s) = G_E(\tau/\tau_E(k)), \quad \tau = t-s, \quad 1/\tau_E(k) \equiv \epsilon^{1/3}k^{2/3}, \tag{23}$$

in the inverse energy transfer range given by Eq. (1).[20] Here, we consider the frequency shift in the inverse energy transfer range when $\delta \equiv \omega_0(\mathbf{k})/\tau_E(k)$ is very small, but finite. We assume that the energy spectrum is given by Eq. (1) to the leading order of small δ. If Eq. (1) is substituted, both the integrations in Eqs. (18) and (19) converge properly at both high and low q, and $A(\mathbf{k})$ and $B(\mathbf{k})$ are given by

$$A(\mathbf{k}) = a/\tau_E^2(k), \quad B(\mathbf{k}) = b\,\omega_0(\mathbf{k})/\tau_E^2(k), \tag{24}$$

where a and b are dimensionless constants of order unity. The first equation in Eq. (24) suggests that the characteristic time scale of G for small β is of the order τ_E. Since $1/\tau_E(k) \gg 1/\tau_E(q)$ for $k \gg q$, (24) gives

$$2A(\mathbf{k}) \gg A(\mathbf{q}), \quad 2A(\mathbf{k}) \gg |C(\mathbf{q})|, \tag{25}$$

for $k \gg q$, in agreement with the first two inequalities of III. Therefore, from Eq. (17), we assume

$$2\,\phi_R(\mathbf{k}) \gg \phi_R(\mathbf{q}), \quad 2\,\phi_R(\mathbf{k}) \gg |\,\phi_I(\mathbf{q})| \sim |\omega_0(\mathbf{q})\tau|, \tag{26}$$

for $k \gg q$, $\delta \ll 1$, and $\tau = O[\,\tau_E(k)]$. Hence, for $k \sim p \gg q$ and $\delta \ll 1$, we have

$$\begin{aligned}\mathrm{Im}\,\theta(-\mathbf{k},\mathbf{p},\mathbf{q}) &\sim \mathrm{Im}\,\theta(-\mathbf{k},\mathbf{k},\mathbf{q})\\ &\sim -\omega_0(\mathbf{q})\int_0^\infty \exp[-2\,\phi_R(\mathbf{k},\tau)]\,\tau\,d\tau.\end{aligned} \tag{27}$$

This is to be compared with Eq. (20). To the first approximation for small δ, we may approximate ϕ_R by $\phi_E \equiv -\ln G_E$, i.e.,

$$\mathrm{Im}\,\theta(-\mathbf{k},\mathbf{p},\mathbf{q}) \sim -\omega_0(\mathbf{q})\int_0^\infty \exp[-2\,\phi_E(\mathbf{k},\tau)]\,\tau\,d\tau.$$

One sees that the imaginary part of Eq. (13) diverges at low q when Eqs. (1), (23), and (27) are substituted. This implies that the dominant contribution to $\mathrm{Im}\,T$ comes from the energy containing range, in agreement with I. Therefore, we need to know about G in the energy containing range. Equations (18) and (19) and the dimensional consideration suggest that

$$A(\mathbf{q}) = B(\mathbf{q})/\omega_0(\mathbf{q}) = O(k_E^2E) \ll 1/\tau_E^2(k), \quad \text{for } k \gg q \sim k_E,$$

where k_E is the characteristic wave number of the energy containing eddies. Hence, we may assume Eqs. (26) and (27) for $q \sim k_E \ll k$.

Under these considerations, from Eq. (22) we obtain

$$\Delta\omega(\mathbf{k}) \sim \frac{I_E}{6}\beta E\,\tau_E^2(k)k_x = \frac{I_E}{6}\frac{\beta E}{\epsilon^{2/3}}\frac{k_x}{k^{4/3}}, \tag{28}$$

Downloaded 19 Oct 2006 to 133.6.32.11. Redistribution subject to AIP license or copyright, see http://pof.aip.org/pof/copyright.jsp

where

$$I_E = \int_0^\infty x G_E^2(x)\,dx, \tag{29}$$

and we have used Eq. (1) with $U(k) \propto E(k)/k$ and Eq. (23) so that

$$\frac{1}{U(k)}\frac{\partial[k^2 U(k)]}{\partial k} = -\frac{2k}{3},$$

and

$$\gamma(k) = \int_0^\infty \exp[-2\phi_E(\mathbf{k},\tau)]\,\tau d\tau = I_E \tau_E^2(k),$$

in which $G_E(\tau/\tau_E) \equiv \exp[-\phi_E(\mathbf{k},\tau)]$. The numerical integration based on the LRA solution for $G_E = \exp(-\phi_E)$ gives $I_E = 0.03$.[20]

B. Enstrophy transfer range (I)

When $\beta = 0$, the LRA gives Eq. (3) and G of the form

$$G(k,t,s) = G_Z[\tau/\tau_Z(k)], \quad 1/\tau_Z(k) = \eta^{1/3}[\ln(k/k_1)]^{1/3}, \tag{30}$$

in the enstrophy transfer range given by Eq. (3).[20]

The frequency shift in the range in which $\delta \equiv \omega_0(\mathbf{k})/\tau_Z(k) \ll 1$ can be estimated in essentially the same manner as above. If Eq. (3) is substituted, both the integrations in Eqs. (18) and (19) diverge at low q. A similar analysis of the enstrophy transfer range in the TFM[8] or LRA[20] shows that

$$A(\mathbf{k}) = a'/\tau_Z^2(k), \quad B(\mathbf{k}) = b'\omega_0(\mathbf{k})/\tau_Z^2(k), \tag{31}$$

where a' and b' are dimensionless constants of order unity. These estimates give Eq. (25) in the enstrophy transfer range. Therefore, we may also assume Eq. (26) in this range. The dominant contribution to the imaginary part of the integration of Eq. (13) comes from nonlocal interactions with small wave numbers, in agreement with Assumption I. By using $\phi_Z \equiv -\ln G_Z$ instead of ϕ_R as the first approximation, we have

$$\Delta\omega(\mathbf{k}) \sim \frac{I_Z}{2}\beta E \tau_Z^2(k) k_x = \frac{I_Z}{2}\frac{\beta E}{\eta^{2/3}}\frac{k_x}{[\ln(k/k_1)]^{2/3}}, \tag{32}$$

where

$$I_Z = \int_0^\infty x G_Z(x)\,dx, \tag{33}$$

and we have used (3) and (30), so that

$$\frac{1}{U(k)}\frac{\partial[k^2 U(k)]}{\partial k} \sim -2k,$$

$$\gamma(\mathbf{k}) = \int_0^\infty \exp[-2\phi_Z(\mathbf{k},\tau)]\,\tau d\tau = I_Z \tau_Z^2(k),$$

in which $G_Z(\tau/\tau_Z(k)) \equiv \exp[-\phi_Z(\mathbf{k},\tau)]$. The numerical integration based on the LRA solution for G_Z obtained in previous studies[14,20] gives $I_Z = 0.13$.

C. Enstrophy transfer range (II)

As shown in Ref. 15, when $\beta = 0$ and $U(q)$ is very large for q in the low wave number range outside the enstrophy transfer range, the energy spectrum may be given by Eq. (4). In this case, $A(\mathbf{k})$ in Eq. (18) may be approximated by

$$A(\mathbf{k}) \sim \tfrac{3}{4}\Omega^2.$$

Therefore, we approximate $G(\mathbf{k},\tau)$ as

$$G(\mathbf{k},\tau) \sim \exp(-\tfrac{3}{4}\Omega\tau^2), \tag{34}$$

in the enstrophy transfer range, in the same spirit as discussed in KH, where the truncated expressions $\phi_R(\mathbf{k}) \sim \nu k^2\tau + A(\mathbf{k})\tau^2$ and $\phi_I(\mathbf{k}) \sim \omega_0(\mathbf{k})\tau + B(\mathbf{k})\tau^3$ are used to evaluate $\theta(-\mathbf{k},\mathbf{p},\mathbf{q})$ in Eq. (14). Strictly speaking, the characteristic time scale of $G(\mathbf{q},\tau)$ is generally not much longer than that of $G(\mathbf{k},\tau)$ for $q \ll k$ in cases where low wave number modes have a large damping factor, as in the runs of Series Z2 as discussed in Ref. 15. However, if one considers the time dependence of $G(\mathbf{q},\tau)$, then an analysis of the integral (14) becomes very complicated. In order to obtain a rough estimate of the integral, we introduce a bold simplifying assumption for small, but nonzero, β that we may neglect the time dependence of $G(\mathbf{q},\tau)$ in estimating the integral (14) and assume III. [Note that if $\phi_R(\mathbf{k})$ is of a magnitude similar to that of $\phi_R(\mathbf{q})$, then neglecting $\phi_R(\mathbf{q})$ may underestimate the exponent in the integrand of Eq. (14) by roughly 1/3.] By using Eq. (34) for $\exp[-\phi_R(k,\tau)]$ and neglecting the time dependence of $G(q,\tau)$ as a first approximation, we then obtain from Eq. (22),

$$\Delta\omega(\mathbf{k}) \sim \frac{\beta E}{6\Omega}k_x, \tag{35}$$

where we have used $U(k) \propto k^{-4}$ in the enstrophy transfer range.

V. NUMERICAL RESULTS FOR $\Delta\omega$

In the following section, we study the frequency shifts $\Delta\omega(\mathbf{k}) \equiv \mathrm{Im}\,T(\mathbf{k})/U(\mathbf{k})$ in the inertial subranges obtained by the numerical simulations of Series E, Z1, and Z2 with $\beta \neq 0$, and compare them with the theoretical estimates obtained in Sec. IV. It may be worthwhile to note that Figs. 2, 6, and 9 show that the energy spectra for $\beta \neq 0$ overlap those for $\beta = 0$ well. This suggests that the effect of nonzero β is not significant regarding the energy spectra in the inertial subranges in the cases under consideration.

In order to obtain the stationary form of $\Delta\omega(\mathbf{k})$ for Series E, Z1, and Z2, we took time averages of $\mathrm{Im}\,T(\mathbf{k})$ and $U(\mathbf{k})$ over the same time interval used to calculate the time-averaged spectra for Series E, Z1, and Z2. Then, we divided the time-averaged $\mathrm{Im}\,T(\mathbf{k})$ by the time-averaged $U(\mathbf{k})$. Note that the time intervals of the averages here are of order $10\zeta_{\mathrm{rms}}^{-1}$. KH calculated $\Delta\omega(\mathbf{k})$ in the same manner, but their time intervals for the averages were limited to the order $\zeta_{\mathrm{rms}}^{-1}$ or so because they only considered freely decaying turbulence. They showed that the fluctuations of the simulated values of $\Delta\omega(\mathbf{k})$ averaged over the short time interval are so large that a detailed quantitative comparison with the theo-

Downloaded 19 Oct 2006 to 133.6.32.11. Redistribution subject to AIP license or copyright, see http://pof.aip.org/pof/copyright.jsp

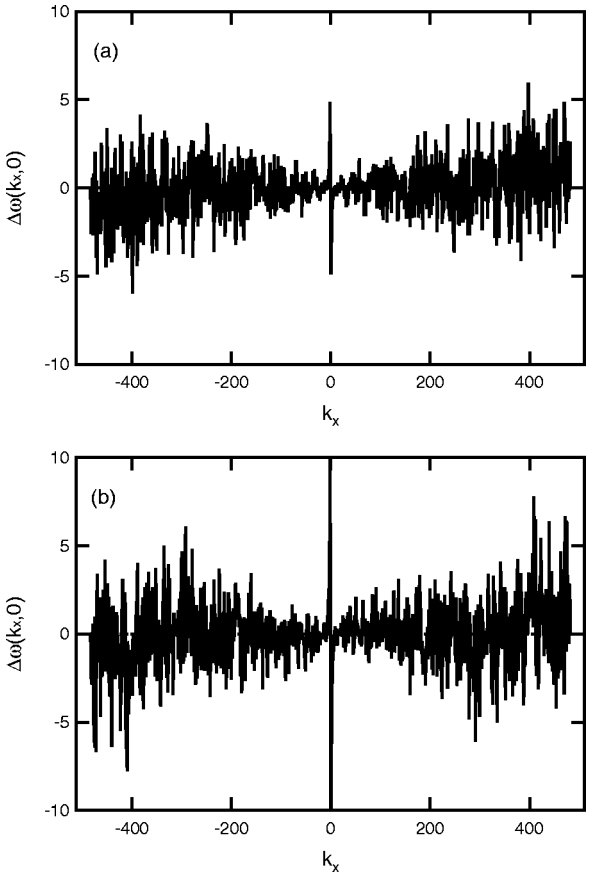

FIG. 12. Plots of $\Delta\omega(k_x,0)$ for Series E with (a) $\beta=5$ and (b) $\beta=10$.

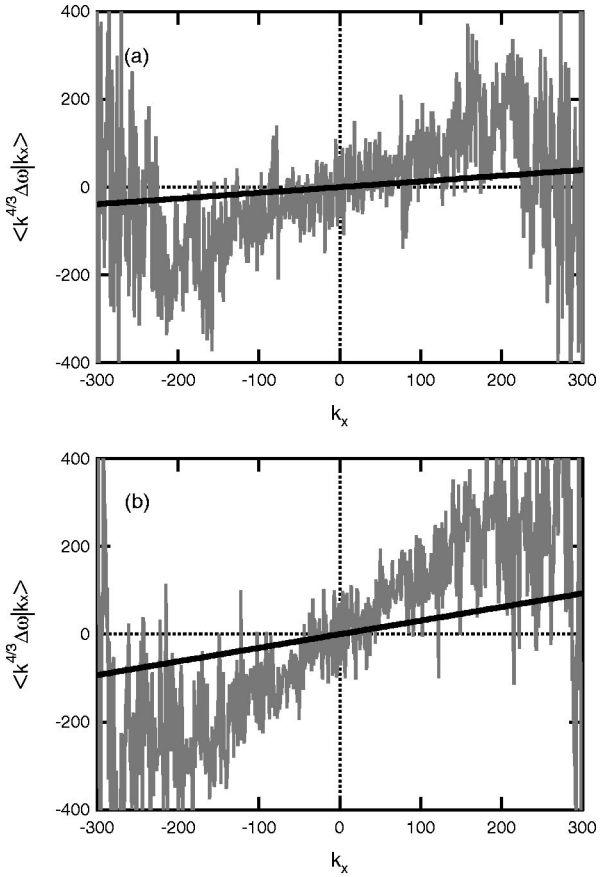

FIG. 13. Plots of $\langle k^{4/3}\Delta\omega|k_x\rangle$ vs k_x for Series E with (a) $\beta=5$ and (b) $\beta=10$ (gray lines), and the theoretical predictions (28) (black lines).

retical estimates is difficult. To make the quantitative comparison easier, we introduce an averaging method in $\mathbf{k}$ space below that considers the simple $\mathbf{k}$ dependence of the theoretical estimates of $\Delta\omega(\mathbf{k})$, i.e., Eqs. (28), (32), and (35).

A. $\Delta\omega$ in the inverse energy transfer range

Figures 12(a) and 12(b) show the time-averaged $\Delta\omega(\mathbf{k})$ at $k_y=0$ for Series E with $\beta=5$ and 10, respectively, as functions of k_x. The fluctuations of the curves in Figs. 12(a) and 12(b) with k_x are so large that both quantitative and qualitative comparisons with the theory seem difficult. The theoretical estimate (28) suggests that $\Delta\omega(\mathbf{k})\propto k_x/k^{4/3}$ and $\Delta\omega(k_x,0)\propto \mathrm{sign}(k_x)|k_x|^{-1/3}$ in the inverse energy transfer range, so that $\Delta\omega$ may be too small in the range to be observed. Note that since $(E,\epsilon)\approx(0.0119, 0.000\,11)$ for $\beta=5$ and $(E,\epsilon)\approx(0.0141, 0.000\,11)$ for $\beta=10$, the prefactors $(I_E/6)\beta E/\epsilon^{2/3}$ of $k_x/k^{4/3}$ for $\beta=5$ and 10 are about 0.13 and 0.31, respectively. Therefore, the values of $\Delta\omega$ in the inverse energy transfer range are too small to be observed in plots such as Fig. 12.

In order to make the quantitative comparison with Eq. (28) easier, we compute $k^{4/3}\Delta\omega$ instead of $\Delta\omega$ itself and define the following average for a fixed integer k_x:

$$\langle k^{4/3}\Delta\omega|k_x\rangle \equiv \frac{1}{N_x}\sum_{\mathbf{p}}{}' \, p^{4/3}\Delta\omega(\mathbf{p}), \tag{36}$$

where $\Sigma'_{\mathbf{p}}$ denotes the sum over $\mathbf{p}=(p_x,p_y)$ satisfying $k_x-\frac{1}{2}\leqq p_x<k_x+\frac{1}{2}$ and $|\mathbf{p}|<300$, and N_x is the number of such $\mathbf{p}$'s. Here, the condition $|\mathbf{p}|<300$ is imposed in order to exclude the effect of artificial forcing in the wave number range $k\in[320, 325]$ from the averaging. Figures 13(a) and 13(b) show that $\langle k^{4/3}\Delta\omega|k_x\rangle$, which still fluctuates with k_x, seems to be roughly proportional to k_x in the inverse energy transfer range, as suggested by Eq. (28). The slopes of the simulated values of $\langle k^{4/3}\Delta\omega|k_x\rangle$ for $\beta=5$ and 10 are of similar order to the theoretical estimates 0.13 and 0.31 obtained by Eq. (28) with $I_E=0.03$, but are steeper somehow. It is worth noting that the time scale of $G(k,t,s)$ in Eq. (23) is inversely proportional to the square root of the universal constant C,[20] so that the integral I_E in Eq. (29) is inversely proportional to C. Use of the simulated value 5.7 instead of the LRA value 7.41 would increase the theoretical estimate by about 30% and the agreement between theory and the simulation would improve slightly.

B. $\Delta\omega$ in the enstrophy transfer range (I)

Figures 14(a) and 14(b) show the time-averaged $\Delta\omega(\mathbf{k})$ at $k_y=0$ for Series Z1 with $\beta=5$ and 10, respectively, as functions of k_x. In agreement with the theoretical estimate (32), the values of $\Delta\omega(k_x,0)$ for $\beta=5$ and 10 are roughly proportional to k_x, which suggests that $\Delta\omega(\mathbf{k})\propto k_x/[\ln(k/k_1)]^{2/3}$ and $\Delta\omega(k_x,0)\propto k_x/[\ln(|k_x|/k_1)]^{2/3}$ in the en-

Downloaded 19 Oct 2006 to 133.6.32.11. Redistribution subject to AIP license or copyright, see http://pof.aip.org/pof/copyright.jsp

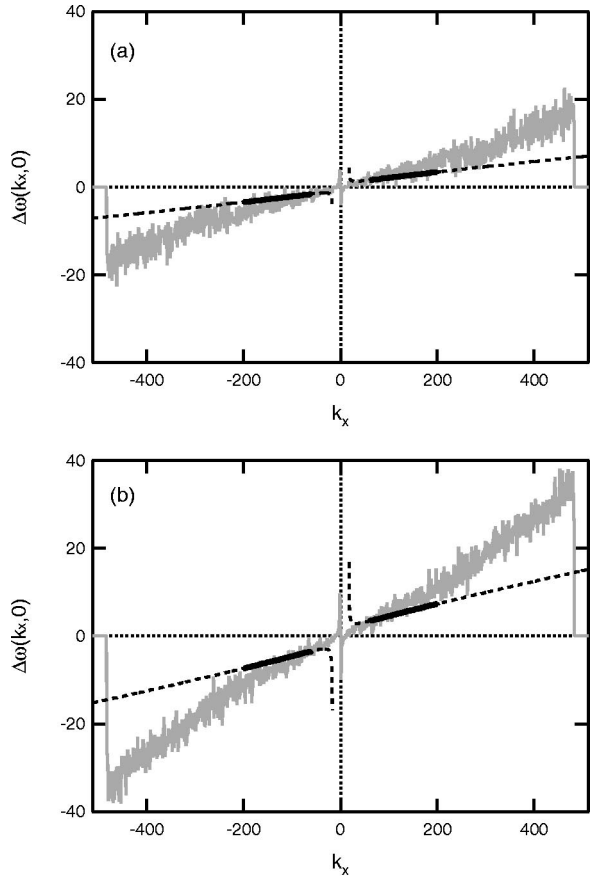

FIG. 14. Time-averaged $\Delta\omega(k_x,0)$ for Series Z1 with (a) $\beta=5$ and (b) $\beta=10$ (gray lines), and the theoretical predictions (32) (thin broken lines); the values of Eq. (32) in the enstrophy transfer range $k\in(60, 200)$ are highlighted with thick solid lines.

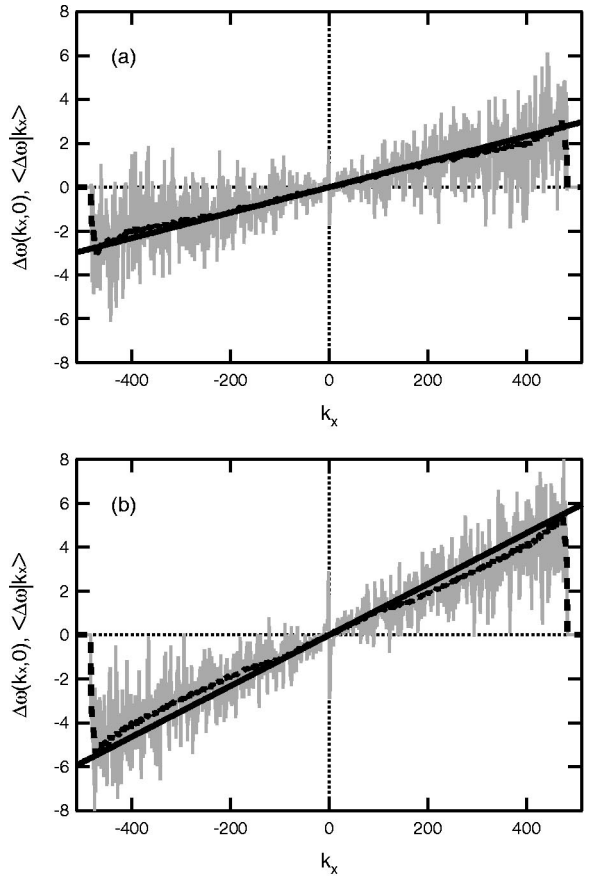

FIG. 15. Time-averaged $\Delta\omega(k_x,0)$ (gray lines) and $\langle\Delta\omega|k_x\rangle$ (broken lines) for Series Z2 with (a) $\beta=5$ and (b) $\beta=10$ as functions of k_x, and the theoretical predictions (35) (thick solid lines).

strophy transfer range of Eq. (3). Since $(E,\eta)\approx(0.0584, 0.466)$ for $\beta=5$ and $(E,\eta)\approx(0.0645, 0.491)$ for $\beta=10$, the prefactors $(I_z/2)\beta E/\eta^{2/3}$ for $\beta=5$ and 10 are about 0.0316 and 0.0674, respectively. In order to determine k_1 in Eq. (32), we applied the same fitting method used to determine C_K and k_1 in Ref. 14 to the data for Series Z1 with $\beta=5$ and 10. The results are $C_K=1.94[1.91, 1.96]$ and $k_1=16.3[12.2, 22.5]$ for $\beta=5$ and $C_K=2.01[1.98, 2.04]$ and $k_1=16.7[12.3, 23.3]$ for $\beta=10$, where the fitting range is $k\in(60, 200)$ and the values in parentheses denote the uncertainty of the measurement results. We also tried the same fitting for the data averaged over $t=60-70$ instead of $t=70-80$ to check the equilibration of Series Z1 and the robustness of the values of C_K and k_1; the results are $C_K\approx1.9-2.0$ and $k_1\approx12-23$, irrespective of the values of β. The simulated values of C_K are in fairly good agreement with the theoretical values (≈1.8) for $\beta=0$[8,20] and those of k_1 are consistent with the theories. These facts support Assumption II. The integral I_Z in Eq. (33) is inversely proportional to the universal constant C_K, so that using these simulated values instead of the LRA value 1.81 would decrease the theoretical estimate roughly 7%. Note that the above uncertainty in the values of k_1 has no significant effect on the estimate of $\Delta\omega$ in Eq. (32).

Although the slope of the simulated $\Delta\omega(k_x,0)$ in Figs. 14(a) and 14(b) is somehow steeper than the theoretical estimate (32), the slopes are of similar order in the enstrophy transfer range $k\in(60, 200)$.

C. $\Delta\omega$ in the enstrophy transfer range (II)

Figures 15(a) and 15(b) show the time-averaged $\Delta\omega(k_x,0)$ and $\langle\Delta\omega|k_x\rangle$ as functions of k_x for Series Z1, respectively, with $\beta=5$ and 10, where $\langle\Delta\omega|k_x\rangle$ is defined in the same way as Eq. (36). Here we have removed the condition $|\mathbf{p}|<300$. The values of $\Delta\omega(k_x,0)$ and $\langle\Delta\omega|k_x\rangle$ for $\beta=5$ and 10 are roughly proportional to k_x. The theoretical estimate (35) suggests that $\Delta\omega(\mathbf{k})\propto k_x$ in the enstrophy transfer range (4). Since $E\approx0.0084$ and $\Omega\approx1.2$, irrespective of the values of β, the prefactors $\beta E/(6\Omega)$ are about 0.0058 for $\beta=5$ and 0.0117 for $\beta=10$. In Figs. 15(a) and 15(b) the theoretical estimate (35) agrees well with the simulated values of $\Delta\omega$.

VI. SUMMARY AND DISCUSSION

Nonlinear interactions between waves and turbulence cause the frequency shift of Rossby waves, $\Delta\omega$. Therefore, $\Delta\omega$ is a measure of the strength of the interactions. We have estimated the frequency shifts of Rossby waves theoretically and numerically in the inertial subranges of β-plane turbulence. The theoretical estimates are based on the LRA, which

Downloaded 19 Oct 2006 to 133.6.32.11. Redistribution subject to AIP license or copyright, see http://pof.aip.org/pof/copyright.jsp

yields energy spectrum (1) in the inverse energy transfer range, and (3) or (4) in the enstrophy transfer range.

A series of numerical simulations with 1024^2 grids points of the forced β-plane turbulence in Sec. III shows the following.

(i) Spectrum (1) in the inverse energy transfer range is obtained in Series E, and $C \approx 5.7$.

(ii) Spectrum (3) in the enstrophy transfer range is obtained in Series Z1 rather than spectrum (2), and $C_{\mathrm{K}} \approx 1.9$ with $k_1 \approx 18$.

(iii) Spectrum (4) in the enstrophy transfer range is obtained in Series Z2, where $A \approx C_N \eta / \Omega^{1/2}$ with $C_N \approx 4.5$.

Result (i) is consistent with Maltrud and Vallis,[12] who obtained similar results with $C \approx 5.8$ in lower resolution numerical simulations. Regarding (ii), similar numerical results were analyzed in Ref. 14, but only for $\beta = 0$. Regarding (iii), the simulated values of $C_N (\approx 4.5)$ for $\beta = 0$, 5, and 10 agree well with the values 4.9 and 4.7 obtained numerically in Refs. 12 and 15, respectively, for $\beta = 0$. As shown in Figs. 2, 6, and 9, the energy spectra for $\beta \neq 0$ agree well with those for $\beta = 0$. This suggests that the β effect is small in the present cases and is not pronounced in the form of the energy spectra in the inertial subranges. In fact, the wavenumber $k_\beta \sim (\beta / 2 u_{\mathrm{rms}})^{1/2}$ at which the nonlinear term in the equation of motion is of the same order as the β term,[1] is much smaller than those in the inertial subranges for the present simulations; the values of k_β for $\beta = 5$ (and 10) are 4.9 (5.5), 2.7 (3.8), and 4.4 (6.3) in Series E, Z1, and Z2, respectively.

For small β, the leading-order expressions of the frequency shifts of Rossby waves in the inertial subranges of Eqs. (1), (3), and (4), are given by Eqs. (28), (32), and (35), respectively. These estimates are for the frequency shift defined by Eq. (8), and derived by using the LRA and some simplifying assumptions. It may be worthwhile to note here that Legras[18] studied the frequency shifts of Rossby waves on a spherical geometry using a different turbulence closure method, and showed that as k increases, $(\Delta\omega)_{\mathrm{L}} / \omega_0$ tends to a constant independent of the energy spectrum, where $(\Delta\omega)_{\mathrm{L}}$ is the frequency shift under his definition. This behavior for large k, which is in good agreement with his low resolution (483 modes) numerical simulations on a rotating sphere, is different from the behavior in Eqs. (28), (32), and (35), as well as that in numerical simulations cited by Holloway,[3] as discussed in Sec. I, where large systematic frequency shifts are seen among shorter waves. It is to be recalled that both the geometry of his flow field and the definition of $(\Delta\omega)_{\mathrm{L}}$, which is based on a closure model, are different from those used in our study, where the geometry is planar and the frequency shift used in deriving the estimates (28), (32), and (35) is defined by Eq. (8). It is also to be noted that the resolution of the numerical simulations on a rotating sphere cited by Holloway[3] (as well as Legras') is presumably low in today's standard, because they were done in the 1980's (their details are not available, for they remain unpublished). It would therefore be interesting to perform numerical simulations of Rossby wave turbulence on a rotating sphere with high enough resolution, and to estimate the frequency shifts in the inertial subranges.

Figure 13 shows that the simulated values of $k^{4/3} \Delta\omega(\mathbf{k})$ of Series E are roughly proportional to k_x in the inverse energy transfer range, in accordance with Eq. (28). From a quantitative point of view, Eq. (28) underestimates the slopes. The use of the simulated value ($C \approx 5.7$) instead of the LRA value ($C = 7.41$) in the theoretical estimate would increase the slopes by about 30%, but still underestimate the value. This discrepancy might be due to anisotropy of the flow field or any coherent structures in large scales. Therefore, we checked the existence of coherent structures of velocity fields and examined the anisotropy of $U(\mathbf{k})$ by comparing the isotropically band-averaged $\hat{k}_x^2 U(\mathbf{k})$ and $\hat{k}_y^2 U(\mathbf{k})$. Contour maps of the stream function showed that flow patterns are dominated by energy containing eddies and are nearly isotropic for Series E with $\beta = 0$ and 5, while zonal jets exist in large scales for the case $\beta = 10$ (figures omitted). The comparison of band-averaged $\hat{k}_x^2 U(\mathbf{k})$ and $\hat{k}_y^2 U(\mathbf{k})$ showed that the difference is large in the energy containing range of Series E with $\beta = 10$ and negligibly small in the inertial range, while it is small throughout the wave number range for the case $\beta = 5$ (figures omitted). The results are consistent with the observed flow patterns. On the other hand, the discrepancies between the simulated values and the theoretical ones observed in Fig. 13 are rather systematic in β. These facts suggest that the effect of anisotropy of the flow field or those of coherent structure in large scales on the discrepancy is not very strong. The role of coherent structure and the effects of high β and strong anisotropy, which were not taken into account in the theory, remain to be studied. However, note that since the time-averaged values of $\Delta\omega(\mathbf{k})$ for Series E fluctuate largely with $\mathbf{k}$ around a small value (~ 0) (see Fig. 12), the qualitative detection of $\Delta\omega$ in the inverse energy transfer range, as in Fig. 13, is difficult without the theoretical prediction in Eq. (28).

As shown in Fig. 14, Eq. (32) predicts the simulated values of $\Delta\omega$ of Series Z1 in the enstrophy transfer range $k \in (60, 200)$ well, while it underestimates $\Delta\omega$ for large k (> 200). Note that the range $k > 200$, in which the enstrophy flux is not constant, as shown in Fig. 7, is outside the enstrophy transfer range. Therefore, Eq. (32) is not thought to apply for $k > 200$. Equations (32) and (3) are a theoretical expression in the enstrophy transfer range for which the enstrophy flux $\eta(k)$ is constant.

The simulated values of $\Delta\omega$ for Series Z2 show quantitatively good agreements with Eq. (35), not only in the enstrophy transfer range $k \in (100, 200)$, but also for large k (> 200), as shown in Fig. 15. In deriving Eq. (35), we neglected the time dependence of $G(\mathbf{q}, t)$ in estimating the integral of Eq. (14) for $\mathbf{p} = \mathbf{k} - \mathbf{q}$ and $k \sim p \gg q$, although the characteristic time scale of $G(\mathbf{q}, t)$ may not be generally much longer than that of $G(\mathbf{k}, t)$ for $q \ll k$ in cases where low wave number modes have a large damping factor, as in the runs of Series Z2 as discussed in Ref. 15. A similar approximation was used to obtain a rough estimate of $C_N = k^3 E(k) \Omega^{1/2} / \eta$, and gives $C_N \approx 2(6/\pi)^{1/2} = 2.76$, which is lower than the simulated value $C_N \approx 4.5$. In contrast to this underestimation, Eq. (35) agrees well with the simulated $\Delta\omega$ in the enstrophy transfer range. An explanation of the differ-

Downloaded 19 Oct 2006 to 133.6.32.11. Redistribution subject to AIP license or copyright, see http://pof.aip.org/pof/copyright.jsp

ence in the performance of similar approximations applied to different problems remains to be explored.

Despite the simplification used in deriving the theoretical estimates of $\Delta\omega$, Eqs. (28), (32), and (35) show fairly good agreement with the simulated values. The expressions (28), (32), and (35) suggest that the frequency shifts of Rossby waves in the inertial subranges, Eqs. (1), (3), and (4), depend in a simple way on the flow conditions at large scales, provided that the β effect is not large. It would be interesting to test the theoretical predictions of the frequency shifts of Rossby waves presented in this paper experimentally or by observation.

ACKNOWLEDGMENTS

The computations were carried out on the VPP5000/56 system at the computer center of Nagoya University. This work was supported by the ''Research for the Future'' Program of the Japan Society for the Promotion of Science under Project No. JSPS-RFTF97P01101.

[1]P. B. Rhines, ''Waves and turbulence on a beta-plane,'' J. Fluid Mech. **69**, 417 (1975).
[2]P. B. Rhines, ''Geostrophic turbulence,'' Annu. Rev. Fluid Mech. **11**, 401 (1979).
[3]G. Holloway, ''Eddies, waves, circulation, and mixing: Statistical geofluid mechanics,'' Annu. Rev. Fluid Mech. **18**, 91 (1986).
[4]Y. Kaneda and G. Holloway, ''Frequency shifts of Rossby waves in Geostrophic Turbulence,'' J. Phys. Soc. Jpn. **63**, 2974 (1994).
[5]R. H. Kraichnan, ''Inertial ranges in two-dimensional turbulence,'' Phys. Fluids **10**, 1417 (1967).
[6]C. E. Leith, ''Diffusion approximation for two-dimensional turbulence,'' Phys. Fluids **11**, 671 (1968).
[7]G. K. Batchelor, ''Computation of the energy spectrum in homogeneous two-dimensional turbulence,'' Phys. Fluids **12**, II-233 (1969).
[8]R. H. Kraichnan, ''Inertial-range transfer in two- and three-dimensional turbulence,'' J. Fluid Mech. **47**, 525 (1971).
[9]D. K. Lilly, ''Numerical simulation studies of two-dimensional turbulence: Part 1. Models of statistically steady turbulence,'' Geophys. Fluid Dyn. **3**, 289 (1972).
[10]U. Frisch and P. L. Sulem, ''Numerical simulation of the inverse cascade in two-dimensional turbulence,'' Phys. Fluids **27**, 1921 (1984).
[11]J. R. Herring and J. C. McWilliams, ''Comparison of direct numerical simulation of two-dimensional turbulence with two-point closure: the effect of intermittency,'' J. Fluid Mech. **153**, 229 (1985).
[12]M. E. Maltrud and G. K. Vallis, ''Energy spectra and coherent structures in forced two-dimensional and beta-plane turbulence,'' J. Fluid Mech. **228**, 321 (1991).
[13]V. Borue, ''Inverse energy cascade in stationary two-dimensional homogeneous turbulence,'' Phys. Rev. Lett. **72**, 1475 (1994).
[14]T. Ishihara and Y. Kaneda, ''Energy spectrum in the enstrophy transfer range of two-dimensional forced turbulence,'' Phys. Fluids **13**, 544 (2001).
[15]Y. Kaneda and T. Ishihara, ''Nonuniversal k^{-3} energy spectrum in stationary two-dimensional homogeneous turbulence,'' Phys. Fluids **13**, 1431 (2001).
[16]E. Lindborg and K. Alvelius, ''The kinetic energy spectrum of the two-dimensional enstrophy turbulence cascade,'' Phys. Fluids **12**, 945 (2000).
[17]Y. Kaneda, ''Renormalized expansions in the theory of turbulence with the use of the Lagrangian position function,'' J. Fluid Mech. **107**, 131 (1981).
[18]B. Legras, ''Turbulent phase shift of Rossby waves,'' Geophys. Astrophys. Fluid Dyn. **15**, 253 (1980).
[19]G. S. Patterson and S. A. Orszag, ''Spectral calculation of isotropic turbulence: Efficient removal of aliasing interaction,'' Phys. Fluids **14**, 2538 (1971).
[20]Y. Kaneda, ''Inertial range of two-dimensional turbulence in a Lagrangian renormalized approximation.'' Phys. Fluids **30**, 2672 (1987).

Downloaded 19 Oct 2006 to 133.6.32.11. Redistribution subject to AIP license or copyright, see http://pof.aip.org/pof/copyright.jsp